

A simplified multi-particle collision dynamics method to simulate microvascular capillary blood flow

Leonor García-Gutiérrez¹; Robert M. Kerr^{1,2}; Ellák Somfai^{3,4,5}; Donald R. J. Singer^{6,7}

¹Mathematics Institute, University of Warwick, Coventry CV4 7AL, United Kingdom; ²Department of Engineering, University of Warwick, Coventry CV4 7AL; ³Centre for Complexity Science, University of Warwick, Coventry CV4 7AL, United Kingdom; ⁴Department of Physics, University of Warwick, Coventry CV4 7AL, United Kingdom; ⁵Institute for Solid State Physics and Optics, Wigner Research Center for Physics, Hungarian Academy of Sciences, P.O. Box 49, H-1525 Budapest, Hungary; ⁶Warwick Medical School, University of Warwick, Coventry CV2 2DX, United Kingdom; ⁷Department of Medicine, Office of Global Health, University of Yale School of Medicine, 15 York Street, 1074 New Haven, CT 06520 USA.

Address for Correspondence:

Leonor Garcia Gutierrez, MSc
Mathematics Institute, Zeeman Building
University of Warwick
Coventry CV4 7AL - UK
Tel: 07531452131
E-mail: l.garcia-gutierrez@warwick.ac.uk

Total word count: 6176.

ABSTRACT

Aims: Most blood flow models are applicable at arterial level but are not designed to reach down to the capillary scale or to represent the deformation of red blood cells (RBC). However, molecular models are too fine to represent the observable scales of a multi-constituent fluid. The aim of this study is to develop and evaluate a method between these two limits capable of simulating capillary blood rheology, and improving our understanding of the role of the microcirculation in cardiovascular disease.

Methods and results: We use a multi-particle collision dynamics method with Andersen thermostat (MPC-AT) to simulate microcirculatory flow through regular and constricted cylindrical capillaries, with erythrocytes modelled as a net of springs on flattened hexagonal prisms. The model is implemented as a C++ serial library accessed through a Python interface. This model results in spontaneous formation of aggregates of RBCs, allows for axisymmetric red cell positioning related to the Fahraeus effect, and permits RBCs to undergo shape transitions as their velocity increases from 3.0×10^{-4} m/s to 9.3×10^{-3} m/s. In the model, RBCs have a higher velocity than plasma. Introducing a local capillary stenosis within the model results in RBC aggregation and a reduction of their velocity (unconstricted vs. stenosis: 4.71×10^{-4} m/s [IQR, $(4.52-4.92) \times 10^{-4}$] vs. 1.38×10^{-4} m/s [IQR, $(1.25-1.70) \times 10^{-4}$]; Wilcoxon signed rank test $P=0.012$, $n=8$).

Conclusions. This multi-particle method demonstrates that only a limited level of detail is needed for a simulation to acquire basic features of the microcirculation, and represents a promising tool for accurate modelling of capillary flow.

Keywords: capillaries, stenosis, risk factors, blood cells, computers.

INTRODUCTION

High blood pressure is a major risk factor for premature cardiovascular death worldwide. Major complications of hypertension include heart failure, acute coronary syndromes, strokes, and other serious vascular diseases. An increase in blood pressure is associated with changes in microvessels (capillaries¹, arterioles² and venules), which make them more resistant to blood flow³. Impairment of the microcirculation may also contribute to the development of hypertension^{4,5,6}. The presence of reduced capillary density (rarefaction) in normotensive individuals with a genetic predisposition to high blood pressure suggests these problems in the microcirculation could play a role in the onset of hypertension, with Levy et al.⁷ suggesting a “vicious cycle”, in which abnormalities in the capillary microcirculation may initiate, maintain and amplify hypertension.

Capillary rarefaction has been observed in patients with borderline hypertension⁵, moderate to severe established essential hypertension^{8,9}, and secondary hypertension¹⁰. This reduction in capillary density may be structural (anatomic absence of capillaries), functional (due to non-perfusion, i.e. blood not being present) or both¹¹, and patients with moderate to severe hypertension have been observed to have both functional and structural capillary rarefaction^{5,9}. Younger individuals with mild elevation of blood pressure are more likely to show functional, but not structural capillary rarefaction⁹, which is consistent with the theory of Prewitt et al.¹² that hypertension-induced vasoconstriction may lead initially to reversible functional rarefaction of capillaries, later followed by irreversible structural rarefaction. Indeed, capillary rarefaction persists after high blood pressure has been controlled with different types of antihypertensive drugs¹³.

Functional rarefaction is associated with endothelial dysfunction, which is both a feature of hypertension, and a biomarker of risk of cardiovascular events¹⁴. Absence of flow induces the death of endothelial cells¹⁵: this might be a link between functional and structural rarefaction. Contributing factors include the aggregation of platelets and margination of white blood cells that occur due to the reduced flow, and activation of cell adhesion molecules, which leads to the activation of apoptotic pathways¹⁶, implicated in structural rarefaction in experimental hypertension¹⁵.

These concepts highlight the importance of studying capillary flow in the context of hypertension, both with regard to potential biomarker development and to gain insight into capillaries as a new treatment target. Key questions include: discerning how the dynamics of flow affects the structure of the capillary, quantifying the resistance that capillaries introduce in the systemic circulation and identifying the nature and impact of established and new cardiovascular risk factors in determining blood micro-rheology. These variables could include macromolecules in plasma, red blood cell mechanical properties such as deformability and stiffness, vessel diameter, tortuosity and other aspects of structure, and the response of the vessel wall to physical, biochemical and cellular stimuli.

Our aim is to develop a simplified but still robust mathematical model within which the complex interactions of different elements affecting blood flow in capillaries can be simulated. As a test of concept, in this paper we use a simulation method known as multi-particle collision dynamics and a simplified model for the red blood cell membrane to study blood flow in capillaries. The first goal is to construct a model of red blood cell flow in a standardised linear cylindrical capillary, then to assess the effects of a local capillary stenosis, to mimic the impact of white cell margination to reduce the diameter of the capillary lumen. To the knowledge of the authors, this is the first time that these methods have been applied to understanding the flow of RBCs through normal and stenosed capillaries.

METHODS

We use a multi-particle collision (MPC) dynamics method to model the microrheology of blood plasma, coupled with a simplified model for the membranes of red blood cells (RBCs).

The MPC methods are a family of particle-based mesoscopic techniques¹⁷ for simulating fluids in the intermediate or mesoscale. These MPC methods can be understood as a modification of direct simulation Monte Carlo (DSMC), a well-established, stochastic, particle-based approach for solving the non-linear Boltzmann equation.

Modelling key system components.

In this work we use the multi-particle collision dynamics method with Andersen thermostat (MPC-AT), as introduced by Allahyarov and Gompper¹⁸ under the name of “random velocity method”. Key components of the system (the solvent, cells in suspension and the boundaries) are modelled using ensembles of “effective particles” (point particles that act merely as momentum carriers), separated into categories. While the particles within each category have different roles and are subject to different interactions, all the particles stream and collide with their neighbours within a collision cell in the same manner, irrespective of their category. The plasma is represented by N point particles of mass m whose positions \mathbf{x}_i and velocities \mathbf{v}_i are continuous variables, with each effective particle representing a collection of real molecules. A coarse grid is used to divide the system into equal cubic collision cells C_j ($j=1, \dots, N_{\text{cells}}$). The method we use, like all MPC algorithms, consists of two steps: a free streaming step and a multi-particle collision step. During the streaming step, all particles (plasma, RBC membrane and cytosol particles) are allowed to move independently according to Newton’s law for a time Δt , according to equations (1) and (2) in Whitmer and Luitjen’s paper¹⁹. The MPC method we use allows the simulations to be done directly in the canonical ensemble by employing an Andersen thermostat (MPC-AT)¹⁸. The Andersen thermostat couples the dynamics of the particles with a heat bath by choosing post collision velocities from a probability distribution at the desired temperature. In this way, the equivalent temperature distribution is well-defined and velocities do not need to be rescaled, in contrast with other models like Stochastic Rotation Dynamics (MPC-SR). The model explicitly includes a temperature-like parameter (effective temperature) that is used to represent macroscopic velocity fluctuations. During the collision step, a random resetting about local mean velocities is performed, drawing the components of the new relative velocities from a Maxwell-Boltzmann distribution^{20,21} of zero mean and variance $k_B T/m$. The velocity of particle i found in cell j transforms according to equation (6) in Gompper et al.’s paper²².

With this division of the system into lattice cells, the collision environment of a given particle depends on the value of any superimposed constant velocity field. This is unphysical, as Galilean invariance would break down. To restore Galilean invariance, a random shift of the grid is performed prior to the collision step²³, by a uniformly distributed random vector with components in the interval $[-a/2, a/2]$.

Representing red blood cells in the model.

We represent the cytoskeleton of the erythrocytes by a mesh of point particles heavier than plasma particles. These particles are placed on the surface of a flattened hexagonal prism, with particles on the bases forming a triangular mesh and those on the sides a rectangular mesh. This prism is a first approximation to the biconcave disc shape of human RBCs. All the particles are connected by linear springs, which are introduced in their unstretched state at the start of the simulation. We represent the cytosol of the RBC by another set of particles, placed in the interior volume of the RBC, of mass comparable to the plasma particles.

Simulating effects of capillary stenosis.

We perform simulations on regular cylindrical capillaries, and cylindrical capillaries with parabolic stenosis, that represent, for example, platelet aggregation and white blood cell margination.

Representing plasma particles in the model.

Plasma particles are “bounced-back” (i.e. their velocity is reversed¹⁹) from the vessel boundary. We use periodic boundary conditions in the direction of the flow. To introduce an interaction with the RBCs, we coat the geometrical wall representing the capillary with a layer of particles of the same type as the RBC membrane, over some wall thickness. Their placement within that volume layer is given by a uniformly distributed random vector. These particles participate in the MPC algorithm with velocities that are drawn from a random normal distribution with zero mean velocity and the same temperature as the system, computed using a Box-Muller transform²⁴. Their velocities are reset to zero after each collision step. These wall particles are set to exert a repulsive force on the particles forming the RBC membrane.

Testing RBC shape transitions in the model.

In order to check whether our model is capable of reproducing human RBC shape deformations, we perform simulations based on a single RBC in a cylindrical capillary, and increase the velocity of the flow over time by incrementing the external force that is applied to all mobile particles to generate the flow (creating an effect comparable to a pressure gradient force).

Testing for the Fåhræus effect.

In microvessels, the haematocrit (volume concentration of RBCs in the blood) is lower than in larger vessels (Fåhræus effect²⁵). Fåhræus argued theoretically that this happens because the mean velocity of the RBCs in the capillaries is higher than the mean plasma velocity. To test whether our model is able to account for this, we record the mean velocity of the plasma at two different points $x_1=30\mu\text{m}$ and $x_2=70\mu\text{m}$ along our model capillary, and compare that with the velocity of the centre of mass of eight different RBCs flowing through a cylindrical capillary. This is equivalent to eight independent experiments for one RBC.

Statistics.

Data are shown as medians with interquartile range (IQR). Results were compared using non-parametric tests, with $P=0.05$ taken as the threshold for statistical significance. In most analyses, we used a sample size of $n=8$, which is a small subset of the large number of data points our numerical simulations generate. The total number of data points we have (across RBCs, experiments and time) is 1716480. However, most of these are not statistically independent as the simulation time-steps are small compared to the characteristic timescales of the flow. A better way to sample that will provide useful statistical errors is to choose times spaced by the time it takes for one lap to be completed. Eight of these times from each of the three simulations were chosen, giving a sample size of 24 velocity data points for RBCs for analysis at a particular position.

RESULTS

Shapes of single red blood cells.

Our tests of a single RBC in a cylindrical capillary show that it tends to position itself perpendicular to the flow (figure 1). As it picks up velocity, its shape changes quickly from its unstressed form to an axisymmetric parachute shape. If the velocity is increased further, the shape then changes to

being torpedo-like. The RBCs undergo great deformations (figure 2, left) and often occupy most of the capillary lumen (figure 2, right).

Effects of capillary stenosis on aggregation and velocity of red blood cells.

Clustering of the RBCs in our simulations with cylindrical capillaries is shown in figure 3. Deformation and clustering of the RBCs become more evident in the presence of a geometrical stenosis (figure 4). The RBCs slow down and aggregate nearing the stenosis (velocity before stenosis: 3.98×10^{-4} m/s [IQR, $(3.36-4.60) \times 10^{-4}$ m/s]; within the stenosis: 1.38×10^{-4} m/s [IQR, $(1.25-1.70) \times 10^{-4}$ m/s]; Wilcoxon signed rank test $P=0.012$, $n=8$, figures 5, 6 and 7), and speed up, then tend to separate as they leave the constriction. This reversible nature of the red cell aggregate is shown in figure 4. We observe that this clustering happens faster as the haematocrit increases (tested with 2 to 12 RBCs), when the pressure gradient force is higher, and with the degree of stenosis.

Relative velocity of red blood cells and plasma in capillaries.

We compare the velocity of the plasma at two different points $x_1=30\mu\text{m}$ and $x_2=70\mu\text{m}$ (start and end of the stenosed region respectively) with the velocity of the centre of mass of eight RBCs (equivalent to eight independent experiments with one RBC) flowing through a cylindrical capillary. The results from our simulations show that RBC velocity (4.88×10^{-4} m/s [IQR, $(4.75-5.03) \times 10^{-4}$ m/s]), is significantly greater than plasma velocity 3.63×10^{-4} m/s [IQR, $(3.31-3.85) \times 10^{-4}$ m/s]; Wilcoxon signed ranks $P=0.012$, $n=8$).

DISCUSSION

We have developed and tested a simplified MPC-AT model of capillary flow, where the only vesicles are RBCs, with membranes modeled by elastic meshes. Despite these simplifications, the model is capable of reproducing the basic features of capillary blood flow. This includes the generation of a “peloton” effect in the RBCs (rouleaux formation) and shape transitions at low and moderate velocities as the RBCs position themselves perpendicular to the direction of flow and develop a parachute-like shape as velocity increases. The Fåhræus effect²⁵ is reproduced by the model, with the RBC velocity greater than the background plasma velocity. We have also quantified the effects of a local capillary stenosis to cause aggregation of red cells and transient reduction in their velocity.

Fåhræus effect.

Fåhræus's explanation of the decrease in average concentration of RBCs in smaller vessels is based on the hypothesis that the RBCs are transported in the axial stream, which is faster than the marginal stream, where the plasma is relegated to flow²⁵. Due to this, the RBCs spend less time in the capillary than the plasma²⁶ and the haematocrit in the capillaries can be reduced to a value of 10-20%²⁷. Our MPC-AT approach captures evidence for this mechanism: we observe that the velocity of RBCs is greater than that for plasma, and provide quantitative data not published before. We also observe that the RBCs tend to travel close to the axis of the cylinder. This has been also observed in more complex MPC models²⁸. Our results using a simpler RBC membrane model confirm this, suggesting that the origin of this effect is more related to microvascular hydrodynamics than to distinctive features of RBC membranes.

Aggregation of red blood cells.

Human erythrocytes aggregate, especially when the blood flow becomes sluggish²⁹ (through stenosed capillaries, for example) forming rouleaux (reversible aggregates in the shape of stacked

coins), or other shapes. Our results, using MPC-AT confirm observations by previous numerical studies using MPC-SR in cylindrical capillaries²⁷, and fluid particle models²⁹.

The observation of rouleaux formation with capillary stenosis is an important qualitative finding. This “peloton” effect is important because it produces a large increase in blood viscosity³⁰, and the formation and disaggregation of RBC clusters is an important mechanism controlling resistance to flow in the capillaries²⁹. Clustering of the RBCs is generated in our simulations even though attractive forces or stickiness factors are not included in the model. RBC aggregation forces are not well understood: Baskurt and Meiselman³¹ state that the two available theories explaining the formation of rouleaux, namely the bridging model and the depletion model, are mutually exclusive. Our results indicate that a RBC aggregate can be formed from the rheology alone, and that this requires neither an interaction between RBCs nor a detailed description of the membrane.

Effects of capillary stenosis on aggregation and velocity of red blood cells.

Multi-particle collision dynamics methods (Stochastic Rotation Dynamics, MPC-SR) have been used before to study the rheology of RBCs in cylindrical capillaries²⁷, and also to study the flow of plasma through a constricted capillary³². Boryczko, Dzwinel and Yuen²⁹ have used a fluid-particle model to study movement of RBCs through a stenosed cylinder. However, to the knowledge of the authors, this is the first time that a MPC-AT method has been applied to the flow of RBCs through a stenosed cylinder, a clinically relevant abnormal capillary geometry.

The accumulation of RBCs in the region of the stenosis in our simulations can be understood as a local increase in blood viscosity enhanced by the stenosed area. This reproduces unpublished experimental video data *in vivo* obtained by one of the authors (DS), and might contribute both to functional and structural rarefaction.

Shapes of single red blood cells.

Human RBCs undergo shape transitions when the velocity of the flow is increased or they pass through constrictions. They maintain their biconcave discoidal shape in slow capillary flows, experiencing a rotation which aligns their plane perpendicular to the direction of flow. Their discoidal shape is elongated in the flow direction. The shapes and orientation of the RBCs oscillate around this stable elongated shape. On increasing the velocity of the flow, the red blood cell shape becomes parachute-like, while a non-axisymmetric slipper-like shape often forms near the transition velocity (at which the RBC shape changes from biconcave to parachute-like). This has been observed in measurements *in vivo*³³, and has been simulated using more complete models which include both the RBC cytoskeleton and the lipid bilayer as an impermeable mesh over a biconcave disc, with additional modelling to keep the area and volume of the RBCs approximately constant throughout the simulation^{34,35,28}.

Our cross-sectional images of RBCs in movement match the above experimental observations³³, and the behaviour of the RBCs in our model at moderate velocities matches the above experimental and numerical observations, without the need to pre-specify this behaviour.

At higher flow velocity, comparable to that observed in large arteries, RBCs in our model become overly deformed, and exhibit oscillations along their longitudinal dimension and parallel to the direction of flow. No slipper-like shapes are observed. This break-down of our model was expected, since we imposed no condition to keep area or volume constant. This therefore establishes a limiting flow velocity for which a more detailed model for the RBC membrane, like those described in the work cited above^{27,28}, would be needed.

Simulation method.

Acquiring a full understanding of blood microflow involves three major challenges: discerning how

the dynamics of the flow affects the structure of the vessel; quantifying the resistance that capillaries introduce in the general circulation; and identifying which variables dominate the determination of blood micro-rheology. These variables could include macromolecules in plasma, red blood cell mechanical properties such as deformability and stiffness, vessel diameter, tortuosity and structure, and the response of the vessel wall to physical and biochemical stimuli. Determining these interactions cannot easily be done by direct *in vivo* investigations alone, as medical data lacks fine spatial and temporal resolution. Therefore, it would be valuable to have robust simulations to help us gain insight into the complex interactions of the multiple elements that affect blood flow in capillaries in health, and in pre-clinical and clinical disease.

Traditional mathematical models for capillary flow are either based on lubrication theories^{36,37} or continuum fluid dynamics methods³⁸. However, it is the rheology of the red blood cells (RBCs) and their interaction with soluble factors and the capillary endothelial cells that fundamentally determines the properties of the blood in microvessels. These methods cannot resolve complex RBC deformations to the necessary level of accuracy, nor account for the important effects of molecular-level details (e.g. thermal fluctuations) on capillary dynamics³⁸. A macroscopic continuum description based on the Navier-Stokes equations (NSE) is not sufficient to resolve the rheology, as NSE treat blood as a homogeneous fluid, not taking into account RBC shape changes that could greatly affect rheology at the capillary level. A microscopic molecular dynamics (MD) description is also not suitable, because the large number of degrees of freedom and the many fine time-steps required make the study of the mesoscopic timescale behaviour currently impractical (one microsecond simulation of a fairly small system would with current methods take several months to complete³⁹). An intermediate approach between the molecular and the traditional fluid descriptions is therefore necessary, which can account for the short time and length-scales present in capillary blood flow. Approaches that have been developed for microfluidics in general include Dissipative Particle Dynamics (DPD), Lattice Boltzmann (LB), Direct Simulation Monte Carlo (DSMC), Smoothed Particle Hydrodynamics (SPH) and Multi Particle Collision Dynamics (MPC)²². The common factor in all these methods is that, in order to attain high computational efficiency, they retain only essential features of the microscopic physics which are of interest for a specific application. All these approaches are essentially alternative ways of solving the equations describing fluid motion, as they are constructed using the same conservation laws and constitutive relations used to derive the NSE.

Among these intermediate scale (mesoscopic) techniques, particle-based methods have the additional advantage that coupling the degrees of freedom of solute molecules with the solvent is easily implemented. This has previously been exploited to study the dynamics of polymers and vesicles in slow flows^{34,40,41,27,22,42}. We have opted for a MPC method, because it is an efficient particle-based algorithm which does not require small time-steps to attain accuracy (unlike MD and DPD), while at the same time providing a simple algorithm that can represent both the hydrodynamics and statistical and thermodynamic fluctuations. Also, the velocities of the particles are continuous in MPC, which results in unconditional numerical stability, unlike LB²².

The efficiency of this MPC approach comes from considering particle interactions only at discrete time intervals, when they are modelled by a multi-particle collision rule²². MPC is a more efficient version of DSMC because the binary collisions are replaced with collisions between groups of particles belonging to a particular collision cell. Although by construction our method is fundamentally a description of a compressible fluid, approximate incompressibility can be imposed^{43,44}. This is desirable because blood plasma is mainly water, which is incompressible.

This MPC method permits derivation of analytical (exact) expressions for transport coefficients

(e.g. viscosity, self-diffusion constant). It also allows coupling with flexible membranes and it has the capability of representing a variety of non-Newtonian factors such as adhesion, both between protein and cells and between cells. These capabilities of the model are particularly important for representing the effects of stenosis of capillaries, typically due to margination of cells (i.e. platelets and white cells)⁴⁵, in response to the molecular and cellular interactions between white blood cells, platelets and capillary endothelial cells⁴⁶.

Our simulations are very sensitive to small changes in the temperature parameter (effective temperature), which differs from the real physiological temperature by several orders of magnitude. Likewise, the plasma viscosity parameter is three orders of magnitude smaller than experimental values. These discrepancies have been observed previously⁴⁷. All other parameters in our simulations match experimental values.

Determining the values of the parameters of a mesoscopic model to make a quantitative comparison with experimental data is not a straightforward task, as the model contains microscopic parameters that are not measurable in the macroscopic system and likewise macroscopic quantities do not appear explicitly in the model. Further work will be needed to elucidate the relationship between the effective temperature and the true temperature of the system.

CONCLUSIONS

MPC-AT is a highly efficient algorithm with the potential for allowing the introduction of a higher level of detail in the interactions between the cell membranes and vessel walls than previously available, without compromising the computational efficiency of the simulations. These characteristics make MPC-AT a useful tool for the study of the microcirculation in health and disease. Increasing the level of detail in our model will improve our ability to obtain physiologically comparable quantitative results. Since the interactions are controlled by elastic potentials between points on the skeletal meshes of the cells and capillary walls, adding further potentials (i.e. interactions) could be used to derive forces that would define the interactions between cellular structures and relevant solutes in the plasma. This level of detail would allow the use of numerous clinically relevant structural and functional parameters (e.g. membrane elasticity and viscosity), that could eventually be used to model observations taken from individual clinical subjects. Study of diseases affecting the properties of the RBC membrane and RBC morphology, including hyperlipidaemia, diabetes and sickle cell disease, could potentially be further modelled by adjusting interaction parameters for cellular skeletons.

The model we use explicitly includes a temperature-like parameter that is used to represent macroscopic velocity fluctuations. Control of the effective temperature would for example allow us to model the influence of vascular and blood adhesion factors in sickle cell disease.

Of particular interest will be the identification from the model of capillary abnormalities as potential biomarkers for early detection of increased risk of cardiovascular disease. A biomarker based on the microcirculation could for example be helpful in predicting risk of hypertension at an early stage, before the onset of established hypertension, and before the development of target organ damage. Our MPC model also has the potential to complement clinical biomarkers in helping to evaluate new treatments targeting the microcirculation⁷, for example aimed at preventing and reversing capillary rarefaction.

FUNDING

This work was supported by “La Caixa” Foundation grant and the “Giving to Warwick” DARO scholarship. Computing facilities were provided by the Centre for Scientific Computing of the University of Warwick.

CONFLICT OF INTEREST

None declared.

REFERENCES

1. Hasan K. M, Manyonda I. T, Ng F. S, Singer D. R, Antonios T. F. Skin capillary density changes in normal pregnancy and pre-eclampsia. *J Hypertens* 2002;**20**(12):2439–43.
2. Cooper A, Heagerty A. M, Others. Blood pressure parameters as determinants of small artery structure in human essential hypertension. *Clin Sci* 1997;**92**(6):551–566.
3. Jung F, Pindur G, Ohlmann P, Spitzer G, Sternitzky R, Franke R. P, Leithäuser B, Wolf S, Park J.-W. Microcirculation in hypertensive patients. *Biorheology* 2013;**50**(5):241–255.
4. Noon J. P, Walker B. R, Webb D. J, Shore a. C, Holton D. W, Edwards H. V, Watt G. C. Impaired microvascular dilatation and capillary rarefaction in young adults with a predisposition to high blood pressure. *J Clin Invest* 1997;**99**(8):1873–9.
5. Antonios T. F. T, Singer D. R. J, Markandu N. D, Mortimer P. S, MacGregor G. A. Rarefaction of Skin Capillaries in Borderline Essential Hypertension Suggests an Early Structural Abnormality. *Hypertension* 1999;**34**(4):655–658.
6. Antonios T. F. T, Rattray F. M, Singer D. R. J, Markandu N. D, Mortimer P. S, MacGregor G. a. Rarefaction of skin capillaries in normotensive offspring of individuals with essential hypertension. *Heart* 2003;**89**(2):175–8.
7. Levy B, Ambrosio G, Pries A, Struijker-Boudier H. Microcirculation in Hypertension: A New Target for Treatment? *Circulation* 2001;**104**(6):735–740.
8. Ciuffetti G, Pasqualini L, Pirro M, Lombardini R, De Sio M, Schillaci G, Mannarino E. Blood rheology in men with essential hypertension and capillary rarefaction. *J Hum Hypertens* 2002;**16**(8):533–7.
9. Cheng C, Diamond J, Falkner B. Functional capillary rarefaction in mild blood pressure elevation. *Clin Transl Sci* 2008;**1**(1):75–9.
10. Vicaut E. Hypertension and the microcirculation: a brief overview of experimental studies. *J Hypertens* 1992;**10**:S59–S68.
11. Serne E. H, Gans R. O, ter Maaten J. C, Tangelder G.-J, Donker A. J, Stehouwer C. D. Impaired Skin Capillary Recruitment in Essential Hypertension Is Caused by Both Functional and Structural Capillary Rarefaction. *Hypertension* 2001;**38**(2):238–242.
12. Prewitt R, Chen I, Dowell R. Development of microvascular rarefaction in the spontaneously hypertensive rat. *Am J Physiol Hear Circ Physiol* 1982;**243**(2):243–51.
13. Penna G. L. D. A, Garbero R. D. F, Neves M. F, Oigman W, Bottino D. A, Bouskela E. Treatment of essential hypertension does not normalize capillary rarefaction. *Clinics* 2008;**63**(5):613– 618.
14. Quyyumi A. A, Patel R. S. Endothelial dysfunction and hypertension: cause or effect? *Hypertension* 2010;**55**(5):1092–4.
15. Levy B. I, Schiffrin E. L, Mourad J.-J, Agostini D, Vicaut E, Safar M. E, Struijker-Boudier

- H. a. J. Impaired tissue perfusion: a pathology common to hypertension, obesity, and diabetes mellitus. *Circulation* 2008;**118**(9):968–76.
16. Kou B, Zhang J, Singer D. R. J. Effects of cyclic strain on endothelial cell apoptosis and tubulogenesis are dependent on ROS production via NAD(P)H subunit p22phox. *Microvasc Res* 2009;**77**(2):125–33.
 17. Malevanets A, Kapral R. Mesoscopic model for solvent dynamics. *J Chem Phys* 1999;**110**(17):8605.
 18. Allahyarov E, Gompper G. Mesoscopic solvent simulations: Multiparticle-collision dynamics of three-dimensional flows. *Phys Rev E* 2002;**66**(3):036702.
 19. Whitmer J. K, Luijten E. Fluid-solid boundary conditions for multiparticle collision dynamics. *J Phys Condens Matter* 2010;**22**(10):104106.
 20. Noguchi H, Kikuchi N, Gompper G. Particle-based mesoscale hydrodynamic techniques. *Europhys Lett* 2007;**78**(1):10005.
 21. Götze I, Noguchi H, Gompper G. Relevance of angular momentum conservation in mesoscale hydrodynamics simulations. *Phys Rev E* 2007;**76**(4):046705.
 22. Gompper G, Ihle T, Kroll D. M, Winkler R. G. Multi-Particle Collision Dynamics: A Particle- Based Mesoscale Simulation Approach to the Hydrodynamics of Complex Fluids. In: Holm C. Kremer K., *Advanced Computer Simulation Approaches for Soft Matter Sciences III*, Springer Berlin Heidelberg, 2009: 1-87.
 23. Ihle T, Kroll D. M. Stochastic rotation dynamics. I. Formalism, Galilean invariance, and Green-Kubo relations. *Phys Rev E* 2003;**67**(6):66705.
 24. Scott D. W. Box-Muller transformation. *Wiley Interdiscip Rev Comput Stat* 2011;**3**(2):177–179.
 25. Fåhræus R, Lindqvist T. The viscosity of the blood in narrow capillary tubes. *Am J Physiol* 1931;**96**(8):562–568.
 26. Pozrikidis C. Computational hydrodynamics of capsules and biological cells. Boca Raton: CRC Press; 2010.
 27. McWhirter J. L, Noguchi H, Gompper G. Flow-induced clustering and alignment of vesicles and red blood cells in microcapillaries. *Proc Natl Acad Sci* 2009;**106**(15):6039–6043.
 28. McWhirter J, Noguchi H, Gompper G. Ordering and arrangement of deformed red blood cells in flow through microcapillaries. *New J Phys* 2012;**14**(8):085026.
 29. Boryczko K, Dzwinel W, A.Yuen D. Dynamical clustering of red blood cells in capillary vessels. *J Mol Model* 2003;**9**(1):16–33.
 30. Fedosov D, Pan W. Predicting human blood viscosity in silico. *Proc Natl Acad Sci* 2011;**108**(29):11772–11777.
 31. Baskurt O. K, Meiselman H. J. Blood Rheology and Hemodynamics. *Semin Thromb Hemost* 2003;**29**(5):435–450.
 32. Bedkihal S, Kumaradas J. C, Rohlf K. Steady flow through a constricted cylinder by multiparticle collision dynamics. *Biomech Model Mechanobiol* 2013;**12**:929–39.
 33. Tsukada K, Sekizuka E, Oshio C, Minamitani H. Direct measurement of erythrocyte deformability in diabetes mellitus with a transparent microchannel capillary model and high-

- speed video camera system. *Microvasc Res* 2001;**61**(3):231–9.
34. Noguchi H, Gompper G, Lubensky C. T. Shape Transitions of Fluid Vesicles and Red Blood Cells in Capillary Flows. *Proc Natl Acad Sci USA* 2005;**102**(40):14159–14164.
 35. Noguchi H, Gompper G. Dynamics of fluid vesicles in shear flow: Effect of membrane viscosity and thermal fluctuations. *Phys Rev E* 2005;**72**(1):011901.
 36. Secomb T, Hsu R, Pries A. A model for red blood cell motion in glycocalyx-lined capillaries. *Am J Physiol Hear Circ Physiol* 1998;**274**(3 Pt 2):1016–22.
 37. Secomb T. W, Skalak R, Özkaya N, Gross J.F. Flow of axisymmetric red blood cells in narrow capillaries. *J Fluid Mech* 2006;**163**:405-423.
 38. Li X, Vlahovska P, Karniadakis G. Continuum and particle-based modeling of shapes and dynamics of red blood cells in health and disease. *Soft Matter* 2013;**9**:28–37.
 39. Durrant J. D, Mccammon J. A. Molecular dynamics simulations and drug discovery. *BMC Biol* 2011;**9**(71).
 40. Watari N, Makino M, Kikuchi N, Larson R. G, Doi M. Simulation of DNA motion in a microchannel using stochastic rotation dynamics. *J Chem Phys* 2007;**126**(9):094902.
 41. Meblinger S. Hydrodynamics of Rod-Like Colloids and Vesicles. Doctoral dissertation; Universität zu Köln; 2008.
 42. Noguchi H. Dynamical Modes of Deformed Red Blood Cells and Lipid Vesicles in Flows. *Prog Theor Phys Suppl* 2010;**184**:364–368.
 43. Ihle T, Tüzel E, Kroll D. M. Consistent particle-based algorithm with a non-ideal equation of state. *Europhys Lett* 2006;**73**(5):664–670.
 44. Tüzel E, Ihle T, Kroll D. M. Constructing thermodynamically consistent models with a non-ideal equation of state. *Math Comput Simul* 2006;**72**(2):232–236. arXiv:0511312v1.
 45. Fedosov D, Fornleitner J, Gompper G. Margination of White Blood Cells in Microcapillary Flow. *Phys Rev Lett* 2012;**108**(2):1–5.
 46. Watts T, Barigou M, Nash G. B. Comparative rheology of the adhesion of platelets and leukocytes from flowing blood: why are platelets so small? *Am J Physiol Heart Circ Physiol* 2013;**304**(11):H1483–94.
 47. Hecht M, Harting J, Ihle T, Herrmann H. Simulation of claylike colloids. *Phys Rev E* 2005;**72**(1):011408.

FIGURE LEGENDS

Figure 1 a-f. How the shape of a RBC changes as its velocity increases (initial velocity 3.0×10^{-4} m/s). RBCs randomly oriented and centred along the axis of a cylindrical capillary of length $50\mu\text{m}$. Strong accelerations ($3\text{-}40 \text{ m/s}^2$) are applied to all particles. From left to right and top to bottom, the RBC goes three times through a capillary of length $50\mu\text{m}$ under an acceleration of 3 m/s^2 . The RBC first positions itself perpendicular to the flow, then adopts an axisymmetric parachute-like shape, whilst its centre of mass velocity increases from 3.0×10^{-4} m/s to 9.32×10^{-4} m/s, with consistent behaviour over all the numerical experiments performed (10).

Figure 2.

Top row: a) and b) Transmission electron microscope images of a red blood cell travelling through a capillary within mammalian pancreatic tissues, images #80308 and #80309 at <http://remf.dartmouth.edu/images/mammalianPancreasTEM/>. Bottom row, left: c) Cross sectional image at $x=100\mu\text{m}$. This is the ninth RBC out of 15, captured in movement at $t=0.0395$ s. The grid shown is a subdivision of the collision grid, used to increase the resolution of the cross-sectional image. Squares that are black, red and blue contain only plasma, membrane and cytosol particles respectively. A lighter colour means there is a minority of particles of another type present. Green squares are occupied by particles of the three types. One square contains at least one cytoplasmic particle which has escaped (no boundary conditions have been imposed on the membrane in this example). Bottom row, right d): Cross sectional image at $x=150\mu\text{m}$. This is the twelfth RBC out of 15, captured at $t=0.2835$ s.

Figure 3.

a) – i) Clustering of RBCs, or rouleaux formation, in a cylindrical capillary of length $100\mu\text{m}$ with time increasing from left to right and from top to bottom. The velocity of the RBCs increases as they cluster (4.46×10^{-4} m/s [IQR, $(4.12\text{-}4.74) \times 10^{-4}$ m/s] to 5.44×10^{-4} m/s [IQR, $(5.03\text{-}5.67) \times 10^{-4}$ m/s] ; Wilcoxon signed ranks $P= 0.028$, $n=6$).

Figure 4.

Simulation of 5 RBCs in a capillary of length $80\mu\text{m}$ with a biochemically inactive stenosed region at $x_c=60\mu\text{m}$, with time increasing from left to right and from top to bottom.

Figure 5.

Component of the velocity in the x-axis (x-velocity) of the centre of mass of RBC #3 as a function of its x-position a stenosed capillary (length $100\mu\text{m}$, stenosis starting at $x=30\mu\text{m}$, maximum at $50\mu\text{m}$ and ending at $x=70\mu\text{m}$). Similar plots were obtained for the other seven RBCs in the simulation. The RBCs slowed down when approaching the stenosis (area between the discontinuous lines) and while within the stenosis, and sped up after exiting it: velocity pre-stenosis 5.33×10^{-4} m/s [IQR, $(3.41\text{-}7.78) \times 10^{-4}$ m/s], in stenosis 1.77×10^{-4} m/s [IQR, $(1.40\text{-}2.03) \times 10^{-4}$ m/s], post-stenosis 8.17×10^{-4} m/s [IQR, $(6.84\text{-}8.80) \times 10^{-4}$ m/s]; Friedman test $P=0.001$, $n=9$. The time gaps omitted (i.e. the empty space between frames) correspond to the time intervals that the RBCs takes to cross the periodic boundary at $x=100\mu\text{m}$. In other words, these four plots are equivalent to consecutive parts of a unique plot representing a capillary of length $400\mu\text{m}$ with choking points at $x= 50, 150, 250$ and $350\mu\text{m}$.

Figure 6.

Averages of the x-velocity vs. x-position plots over the eight RBCs, for the 2nd and 3rd lap through the capillary, i.e. averages of the frames on the second/third column in figure 5. SEM error bars are displayed.

Figure 7.

Comparison of the x component of the velocity of RBCs in a) a cylindrical capillary of length 100 μm and diameter 10 μm (left), and b) in a stenosed capillary (right). The stenosed example presents the same geometry, with a stenosis starting at 30 μm and ending at 70 μm , with maximum constriction placed at 50 μm . Three simulations were run long enough for the eight RBCs of diameter 8 μm to complete between 2 and 2.5 laps through a modelled capillary. Bars represent the median x-velocities, with 95% confidence interval bars. Friedman tests were run in each case, with no statistical difference found in the cylindrical case ($P=0.417$, $n=8$), and a significant difference in the constricted vessel ($P=0.0003$). Pair-wise post hoc Wilcoxon signed ranks tests with a Bonferroni adjustment were run, showing a significant reduction in x-velocity within compared to before entry to the stenosis ($P=0.012$) and a significant increase in x-velocity for red cells after the stenosis, compared to the velocity both before entry to ($P=0.012$) and within the stenosis ($P=0.012$, $n=8$).

Figure 1

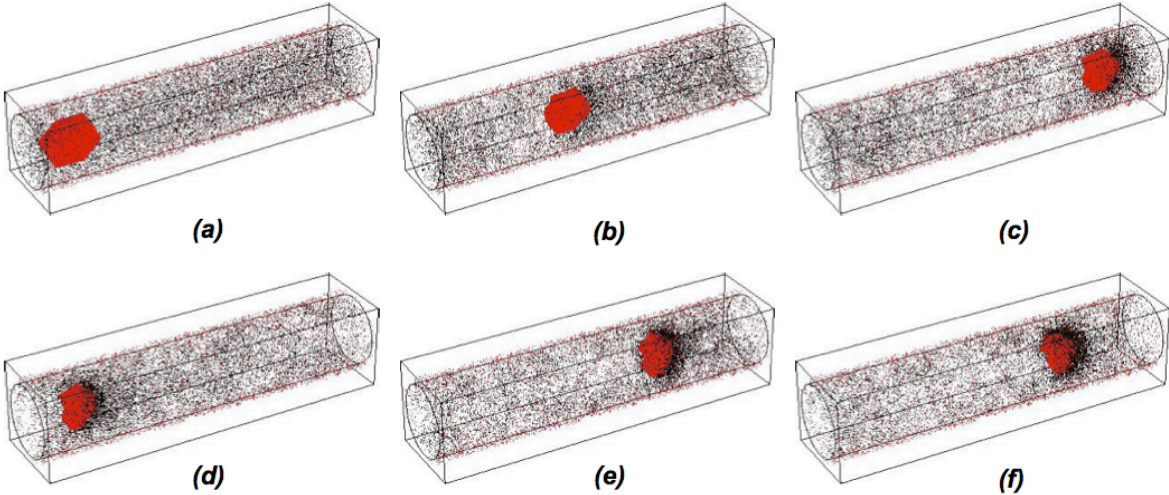
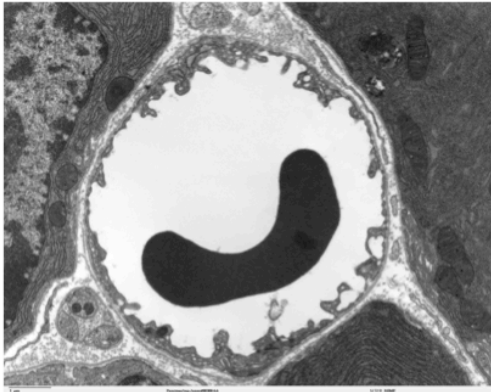
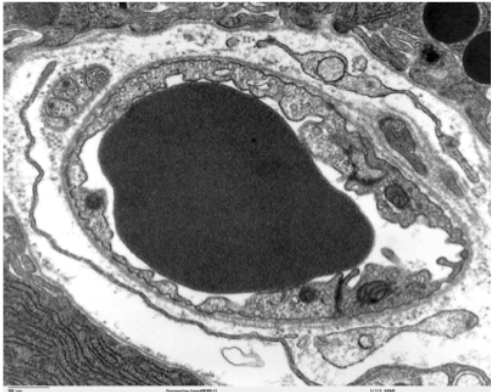


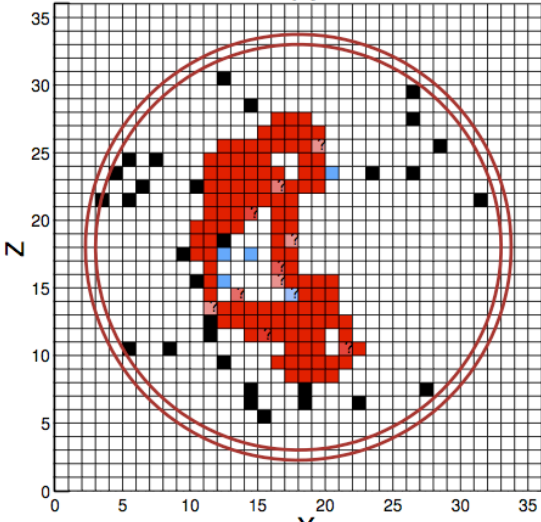
Figure 2



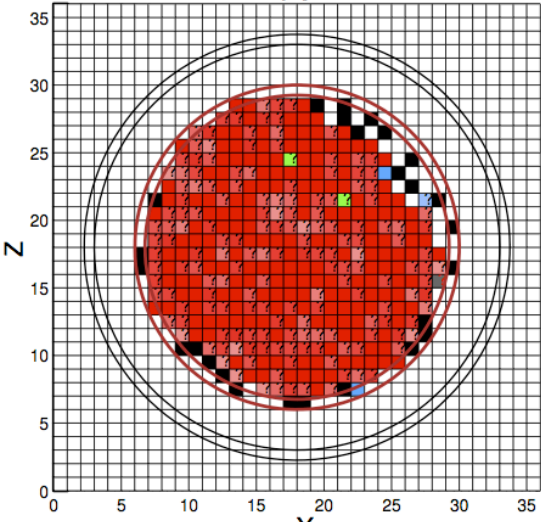
(a)



(b)



(c)



(d)

Figure 3

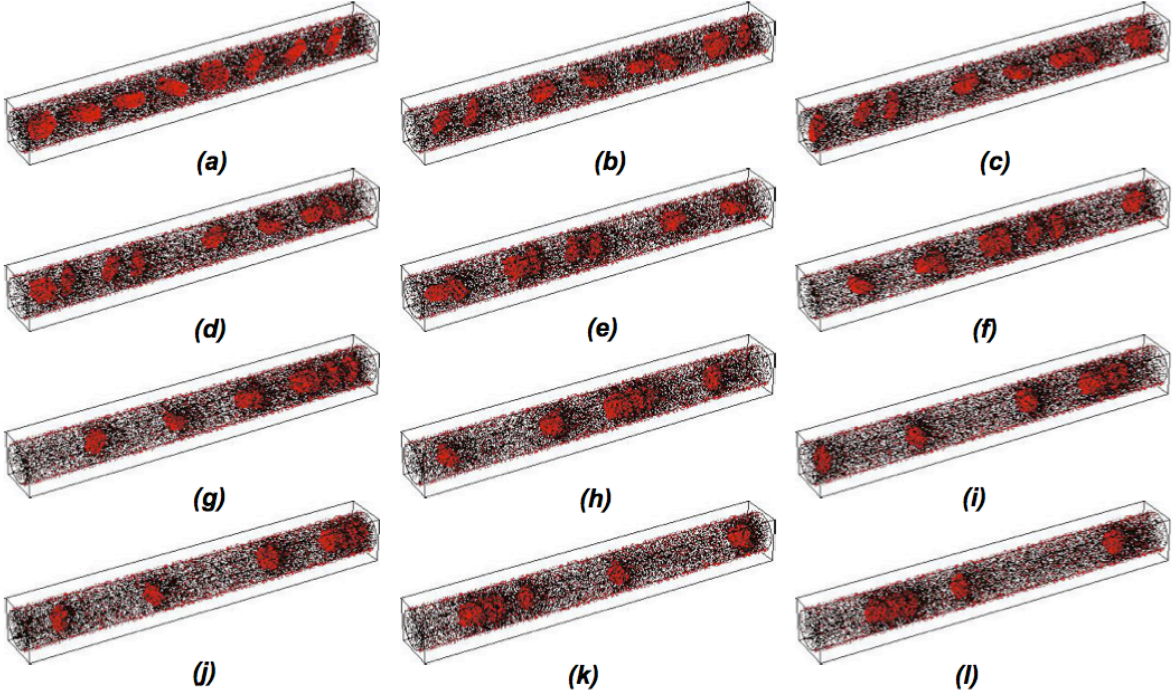


Figure 4

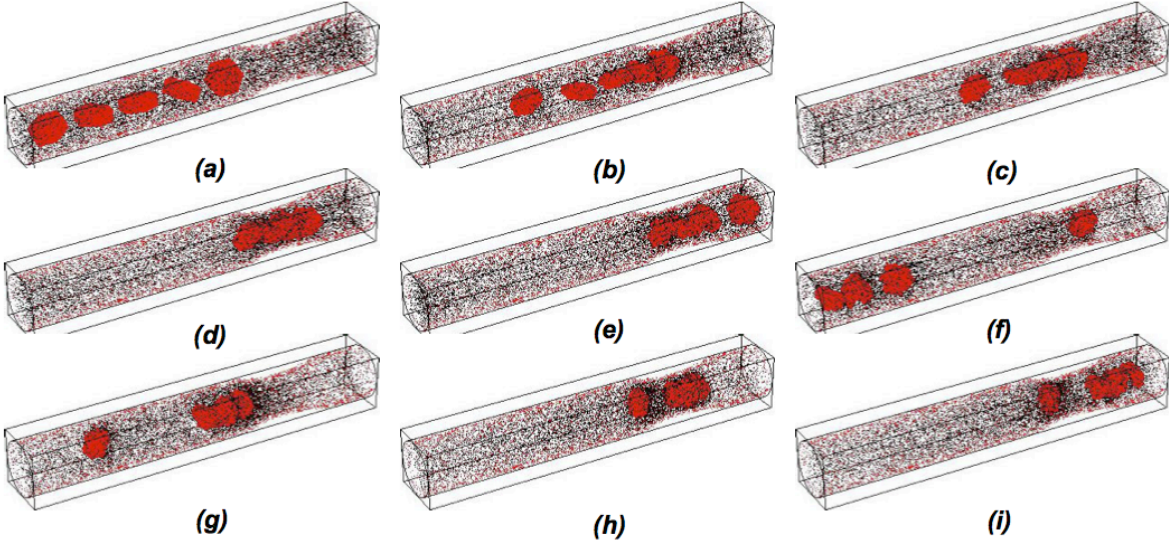


Figure 5

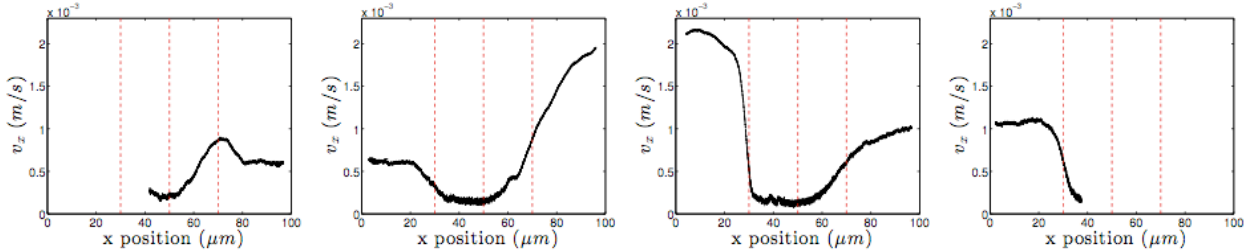


Figure 6

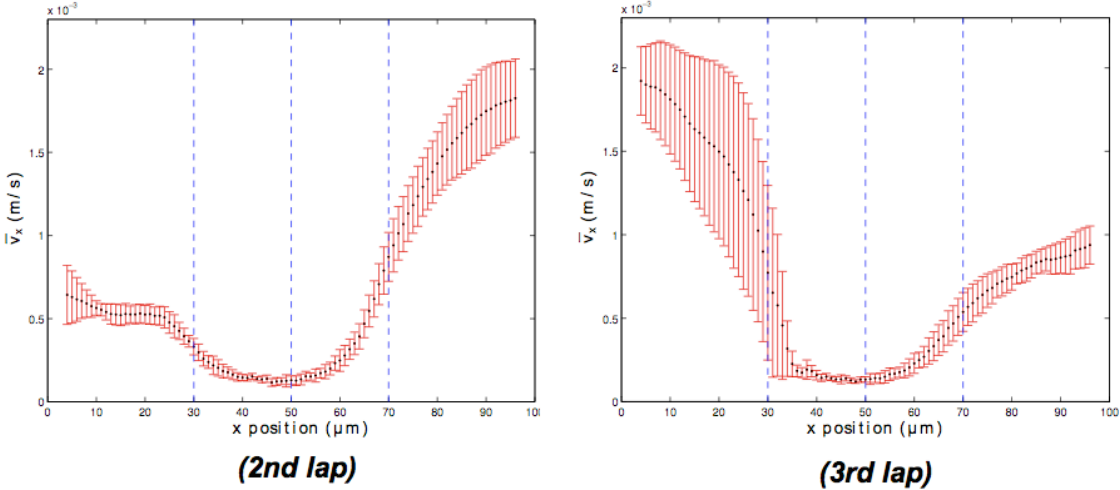


Figure 7

